Research Article | Vol. 29, No. 7 / 29 March 2021 / Optics Express 10374
Optics EXPRESS

Strongly resonant silicon slot metasurfaces with symmetry-protected bound states in the continuum

J. F. ALGORRI,[1,*] F. DELL'OLIO,[2] P. ROLDÁN-VARONA,[1] L. RODRÍGUEZ-COBO,[3] J. M. LÓPEZ-HIGUERA,[1,3,4] J. M. SÁNCHEZ-PENA,[5] AND D. C. ZOGRAFOPOULOS[6]

[1]*Photonics Engineering Group, University of Cantabria, 39005 Santander, Spain*
[2]*Department of Electrical and Information Engineering, Polytecnic University of Bari, 70125 Bari, Italy*
[3]*CIBER-bbn, Instituto de Salud Carlos III, 28029 Madrid, Spain*
[4]*Instituto de Investigación Sanitaria Valdecilla (IDIVAL), 39011 Santander, Spain*
[5]*Department of Electronic Technology, Carlos III University, Madrid 28911, Spain*
[6]*Consiglio Nazionale delle Ricerche, Istituto per la Microelettronica e Microsistemi (CNR-IMM), Roma 00133, Italy*
[*]*algorrijf@unican.es*

Abstract: In this work, a novel all-dielectric metasurface made of arrayed circular slots etched in a silicon layer is proposed and theoretically investigated. The structure is designed to support both Mie-type multipolar resonances and symmetry-protected bound states in the continuum (BIC). Specifically, the metasurface consists of interrupted circular slots, following the paradigm of complementary split-ring resonators. This configuration allows both silicon-on-glass and free-standing metasurfaces and the arc length of the split-rings provides an extra tuning parameter. The nature of both BIC and non-BIC resonances supported by the metasurface is investigated by employing the Cartesian multipole decomposition technique. Thanks to the non-radiating nature of the quasi-BIC resonance, extremely high Q-factor responses are calculated, both by fitting the simulated transmittance spectra to an extended Fano model and by an eigenfrequency analysis. Furthermore, the effect of optical losses in silicon on quenching the achievable Q-factor values is discussed. The metasurface features a simple bulk geometry and sub-wavelength dimensions. This novel device, its high Q-factors, and strong energy confinement open new avenues of research on light-matter interactions in view of new applications in non-linear devices, biological sensors, and optical communications.

1. Introduction

The study of periodic subwavelength structures has attracted much attention in recent years. Such structures can be broadly classified in three categories, namely metamaterials (MM) [1], photonic crystals (PhC), and high contrast metastructures (HCM) [2]. The main difference between these types of structures is their operating principle. While the MM properties are the result of local resonances of its subwavelength elements, PhC and HCM are based on Bragg resonances of the structure as a whole. Besides, PhC and HCM differ in their design approaches, theoretical analyses, and photonic applications, and therefore remain as distinct research topics [2]. One advantage of MM is that they may behave like a bulk material with engineered permeability and permittivity, thus achieving unusual optical properties. Specifically, two-dimensional MM, known as metasurfaces (MS), have gained increased interest due to their interesting properties, compact size, and simpler fabrication [3–8]. These structures are composed of subwavelength-scale optical resonators arranged at the interface between two media. Their local resonances and their collective interactions are capable of modifying the properties of propagating electromagnetic

#415377 https://doi.org/10.1364/OE.415377
Journal © 2021 Received 17 Nov 2020; revised 23 Jan 2021; accepted 2 Mar 2021; published 18 Mar 2021

Optics EXPRESS

waves, such as, amplitude, phase, polarization, and group delay. In addition, depending on the design, dielectric or metallic subwavelength particles can control light scattering and light-matter interactions in both resonant and non-resonant regimes.

In the past decade, all-dielectric MS composed by high refractive index materials have attracted equal or more interest than their metallic counterparts, as they do not suffer from ohmic losses and allow for the excitation of Mie-type magnetic and electric resonant multipole modes. Based on this concept, numerous metasurfaces have been extensively used in a broad range of applications: to achieve arbitrary reflection/refraction [9–11], wavefront control and lensing [12,13], control of light emission [14], photoluminescence [15], polarization control [16], generation of vortex beams [17], sensing [18,19], microwave waveguide design [20], ultra-high quality factor resonant response [21], highly-selective filtering [22,23], or enhancement of nonlinear processes [24,25]. The field has considerably expanded during these past years and some of the most promising achievements are reported in Refs. [26–30]. The traditional building blocks of dielectric MS have been cubes, disks, rods, or other particles of arbitrary geometrical shapes. While in the case of HCM and PhC the building blocks can have a refractive index lower than that of the surrounding material (mesh-type) or the opposite (island-type), the most common MS proposals are based on island-type configurations.

In this work, we propose a novel type of MS based on building blocks of slot geometrical shapes (a mesh-type MS), specifically complementary split-ring resonator (CSRR) ultrathin slots, which can be etched in a silicon layer by standard techniques, such as electron-beam lithography or reactive ion etching. Contrary to metasurfaces based on silicon-SRR patterned on substrate [18], we demonstrate that the MS supports at telecom near-IR wavelengths strong multipolar resonances, such as toroidal quadrupoles, localized in parts of the silicon slab, which are separated by the air-CSRR. Their multipolar nature is investigated by means of the Cartesian multipole decomposition technique (CMDT).

Furthermore, by introducing a degree of asymmetry in the structure of the slotted CSRR, it is shown that a quasi-BIC is excited by an impinging planewave, as earlier proposed in a significantly different context, namely resonant metallic MS at microwave frequencies [31]. The quality factor of the quasi-BIC resonance can be controlled by adjusting the asymmetry parameter, as demonstrated by Fano curve fitting of the simulated MS transmittance spectra and by an eigenfrequency analysis. The impact of optical absorption losses on the achievable quality factors is moreover investigated. Additional advantages of the proposed MS are the possible operation in free-standing configuration (key to maintain some important resonant characteristics of dielectric MS) and the straightforward scaling of the design to other parts of the electromagnetic spectrum (taking advantage of the low dispersion of silicon). This novel approach opens new avenues of research in resonant periodic structures and more precisely in dielectric MS for narrowband filtering, sensing, or the enhancement of non-linear processes.

2. Multipolar resonances in slot metasurfaces

One of the most exotic multipole families recently investigated has been the toroidal multipoles. The simplest member of this class, i.e., the toroidal dipole (TD), is a localized electromagnetic excitation formed when current flows in a solenoid bent into a torus. Depending on the polarization current, magnetic or electric TD or higher-order multipoles, such as toroidal quadrupoles (TQ) are generated. Although toroidal multipoles exist in nature, they are hard to measure as they usually overlap with and are screened by other much stronger multipoles.

The CMDT is the best technique for the theoretical identification of the nature of resonant multipolar modes and it has been widely employed in electromagnetics for the study of light-matter interaction [32]. For instance, this technique has been used to find toroidal moments causing the so-called anapole state [33], to investigate non-spherical nanoparticles [34], trimers [35],

Optics EXPRESS

quadrumers [36–38], nanohole silicon MS [39] and so forth. Here, we employ the CMDT in order to specify the multipolar nature of the resonances observed in the MS transmittance spectra.

Experimentally, the first demonstration of a TD was in a metallic MM in the microwave range [40]. After that, other designs based on split-ring resonators have been demonstrated at THz and visible range [41,42]. Despite the fact that TD are not readily measurable in individual dielectric particles [43], strong toroidal response has been recently demonstrated around 10 GHz [35,44] and 100 GHz [45] in all-dielectric MS. Some example applications of toroidal MS are cloaking [46], nanolasing [47], photoluminescence [48], and enhancement of nonlinear effects [49,50]. As it happens with MS in general, the field has considerably expanded during these past years so the reader is referred to the review studies of Refs. [51–53].

2.1. Near-infrared optical response of the silicon CSRR metasurface

The proposed MS is composed of a periodic array of CSRR slots etched in a thin silicon layer, as shown schematically in Fig. 1. The MS can be fabricated by depositing a polycrystalline silicon film on an optically thick glass substrate by means of low pressure chemical vapor deposition [54] and subsequent patterning of the silicon layer via standard electron-beam lithography (EBL) or reactive ion etching in order to etch the CSRR slots [55]. The structural parameters are characterized by the CSRR width s, its inner diameter w, the distance between adjacent CSRR g, and the silicon layer thickness h. According to this definition, the pitch of the periodic square array is equal to $P = w + g + 2s$. The CSRR are interrupted by two narrow silicon gaps of size t and an additional asymmetry parameter t_x, which reduces the arc length in one half of the CSRR, thus breaking the symmetry of the structure. This is key to the generation of quasi-BIC resonances, as it will be demonstrated in Section 3. Since the MS is based on the complementary pattern of etched SRR, the silicon layer retains its continuity, thus allowing, in principle, for the fabrication of the structure in both free-standing and substrate-supported structures.

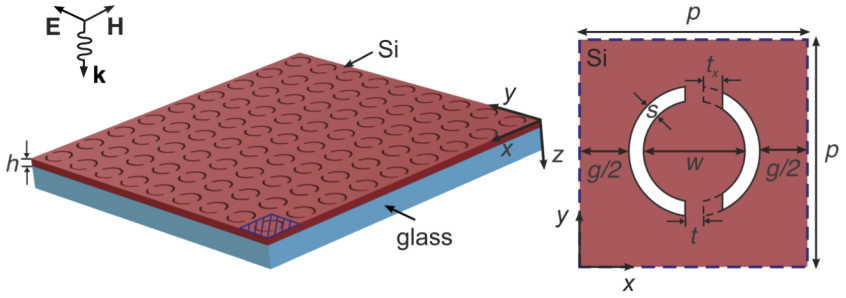

Fig. 1. Schematic diagram of the proposed all-dielectric slot metasurface. The slots are etched as split rings in a thin silicon layer. The symmetry of the structure is broken by introducing an asymmetry parameter t_x, which reduces the length of one CSRR arc and breaks the symmetry of the structure.

To obtain the optical response of the MS, i.e., the power reflectance, absorptance, and transmittance spectra, a high-speed, open-source electromagnetic solver is used, which implements the rigorous coupled-wave analysis (RCWA) [56–59]. As a starting point, the structural parameters are selected to produce strong resonances in the vicinity of $\lambda = 1.55$ μm, that is the third near-infrared (NIR) telecommunications window. Despite this, the structure can be scaled to work in other spectrum regions due to the low dispersion of silicon. In what follows, the material dispersion of silicon was taken into account [60] and the planewave is y-polarized and normally impinging on the MS.

As a first case, we consider a symmetric structure ($t_x = 0$) according to the definition of Fig. 1. The thickness of the silicon layer is adjusted at $h = 232$ nm so that the layer's transmittance is

Optics EXPRESS

maximized at the target wavelength of 1.55 μm. The Fabry-Perot transmittance of the thin silicon layer provides the background of the MS optical response and it is not affected by the CSRR geometrical parameters. A glass substrate is considered with a refractive index of 1.52, as in this NIR scenario the MS is too thin to work in free-standing configuration. However, a scaled version of the MS at THz frequencies, where high-resistivity floating-zone silicon has minimal losses with an only slightly lower refractive index, could be mechanically robust even without a substrate as the required silicon layer thickness is from tens to hundreds of microns.

The MS geometrical parameters are selected as w = 496 nm and g = 240 nm, while the gap t and the CSRR slot width s are free parameters. The results are summarized in Fig. 2. As it can be observed, in all cases examined the MS supports two strong resonances in the spectral window under investigation. When a free-standing silicon MS is considered, namely with a substrate index n_s = 1, the two resonances are closer, as observed in Fig. 2(a) for t = 100 nm and s = 25 nm. The presence of the glass substrate does not suppress these two resonances, but red-shifts their resonant wavelengths, such that the spectral distance between them is increased. The gap width t has a small impact on the MS optical response and it can be used as a parameter to fine-tune the spectral position of the two resonances, as shown in Fig. 2(b). In fact, it is observed that even in the case of t = 0, i.e., when the slots form continuous rings, the same two resonances are observed. Therefore, for their excitation it is not necessary that the slotted rings are split. Their nature is investigated in more detail in Section 2.2. The CSRR width s plays a more critical role, which is evidenced in Fig. 2(c). Thinner slots lead to higher field confinement and thus resonances with increased quality factor (narrower linewidth). In addition, as the slot width is further reduced, the two resonances become spectrally closer.

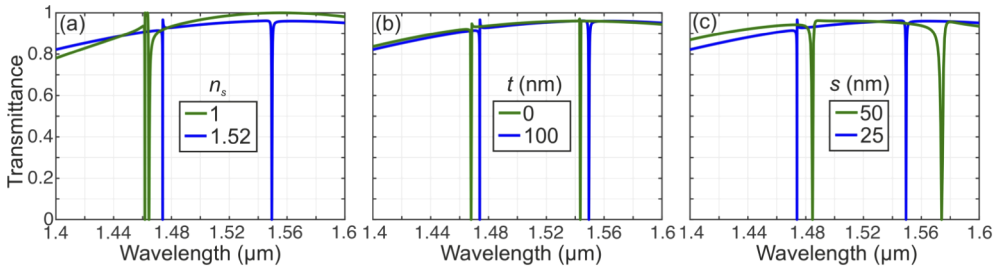

Fig. 2. Transmittance of the investigated silicon CSRR-MS for: (a) free-standing vs. substrate-supported MS, (b) substrate-supported MS with and without silicon gaps, (c) substrate-supported MS for different CSRR slot widths. In all cases, unless stated differently: w = 496 nm, h = 232 nm, g = 240 nm, t = 100 nm, s = 25 nm, and t_x = 0 nm.

2.2. *Electromagnetic field profiles and multipole decomposition of the resonant modes*

In order to elucidate the physical origin of the two observed strong resonances the electromagnetic fields in the MS were simulated at the resonant wavelengths. The 3D finite element method (FEM) was used, implemented in the commercial software COMSOL Multiphysics. The mesh was composed of tetrahedral quadratic elements with maximum size $\lambda_m/7$, where λ_m is the wavelength in each medium. The mesh in the slot region was refined in order to secure convergence of the results. The field profiles were normalized with respect to the amplitude of the impinging planewave, such that the field enhancement factor is directly assessed.

The analysis was complemented with the CMDT, by expanding the polarization current in silicon, which was calculated in the MS unit cell and at the corresponding resonant wavelengths. Then, the relative scattering power P_{sc} of the dipole and quadrupole moments was derived. The total electric dipole and quadrupole moments are composed of the interference of Cartesian electric and toroidal moments, whose scattering power is separately calculated as described

Optics EXPRESS

in Refs. [20,45]. Since the employed CMDT is formulated for scatterers embedded in a homogeneous medium, the free-standing configuration studied in Fig. 2(a) was selected as the case study. However, it has been confirmed, by inspecting the corresponding field profiles, that the multipolar nature of the resonant modes does not change for the case of the glass-backed metasurface.

The results for the two resonant modes at $\lambda^{l}_{\mathrm{res}}$ = 1.4602 μm and $\lambda^{h}_{\mathrm{res}}$ = 1.4643 μm are summarized, respectively, in Fig. 3(a)-(c) and Fig. 3(d)-(f). In the first case, the electric field is polarized almost exclusively in the MS plane, as evidenced in Fig. 3(a) and (b). The observed loops of displacement currents, calculated in the *xy*-midplane of the MS, as well as those of the magnetic field in the transverse *xz*-plane, are a characteristic fingerprint of toroidal multipoles [33]. The field arrows are plotted in logarithmic scale in order to avoid screening their pattern by the strong fields in the slot CSRR. Indeed, the CMDT reveals that the dominant multipole contribution of the investigated resonant mode is the electric quadrupole stemming from a strong TQ moment.

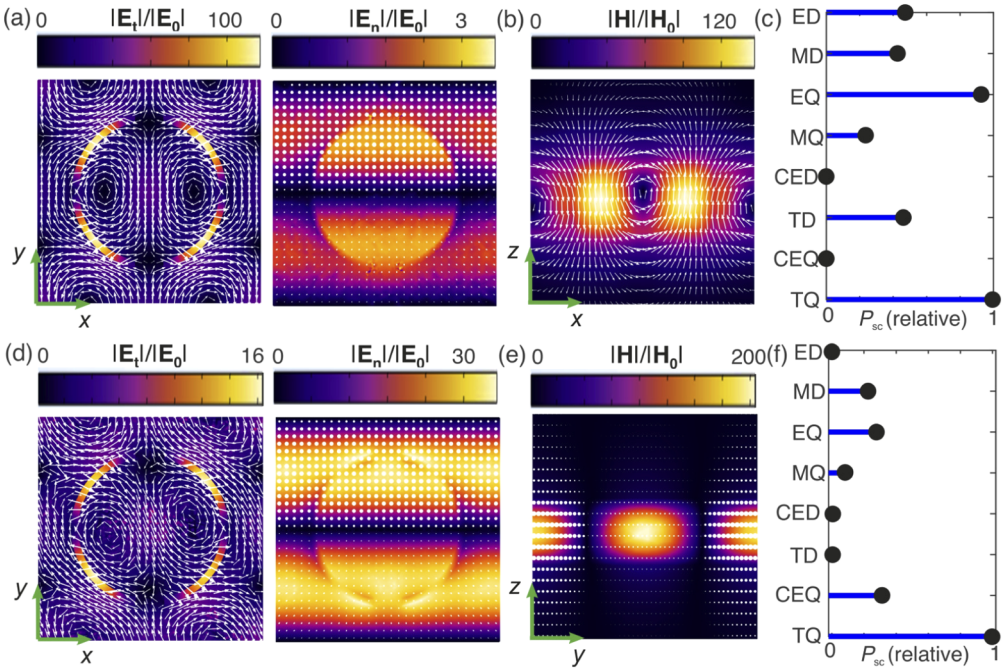

Fig. 3. (a) Electric, (b) magnetic near-field profiles and (c) relative multipole scattering power for the resonance at $\lambda^{l}_{\mathrm{res}}$. (d) Electric, (e) magnetic near-field profiles and (f) relative multipole scattering power for the resonance at $\lambda^{h}_{\mathrm{res}}$. The tangential $\mathbf{E_t}$ and normal $\mathbf{E_n}$ electric field components with respect to the *xy*-plane are plotted separately. The structural parameters are as in the free-standing case studied in Fig. 2(a). Multipole definition: ED-electric dipole, MD-magnetic dipole, EQ-electric quadrupole, MQ-magnetic quadrupole, CED-Cartesian electric dipole, TD-toroidal dipole, CEQ-Cartesian electric quadrupole, TQ-toroidal quadrupole.

The second resonant mode was found to exhibit a hybridized multipolar signature, as evidenced both by the mixed, tangential and normal, polarization of the electric field in the MS midplane and by the multipole analysis. A strong TQ contribution is observed, whose scattering power is however comparable to that of the magnetic dipole. In both cases of the resonant modes there is significant field confinement in the CSRR slots, which is fundamental for the excitation of strong resonances, as observed in the corresponding transmittance spectra of Fig. 2(a).

Optics EXPRESS

3. Bound states in the continuum in slot silicon metasurfaces

The existence of bound states in the continuum was first proposed nearly a century ago in the context of quantum mechanics [61]. This phenomenon consists in waves that stay localized while coexisting with radiating waves in the continuous spectrum [62]. Being a general wave phenomenon, it can be observed in water, acoustic and electromagnetic waves. In the latter case, BIC can dramatically reduce the radiation from optical resonators, since a true BIC has infinite Q-factor. The first experimental demonstration was in 2011 [63], opening up new avenues of research in nanophotonics. The main limitation is that BIC can be produced only in ideal lossless infinite structures or for extreme values of parameters. Despite this, BIC can be probed as quasi-BIC when the Q-factor and resonance linewidth become finite [64]. Recently, they have been demonstrated in various photonic structures as for example, photonic crystal slabs [65–68], optical waveguides and fibers [69,70], metasurfaces [71–74], isolated subwavelength dielectric particles [75], and nanodisks [76]. The envisaged applications are numerous, including among others sensing [77,78], the enhancement of non-linear processes [79], imaging [80], and lasing [81].

The most common way to observe BIC is by breaking the symmetry in systems where the coupling between some resonances to the radiation modes is not allowed due to symmetry or separability [82]. Such systems exhibiting reflection or rotational symmetry can have a bound state embedded in the continuous spectrum of modes of different symmetry class, making the coupling forbidden as long as the symmetry is preserved [62]. In this section, we demonstrate that the proposed metasurface is capable of supporting quasi-BIC by symmetry breaking. To do so, several options are in principle possible, e.g., by accommodating CSRR of different size in the unit cell, introducing an offset of the silicon gap in both or one side, or by shortening the arc length in one part of the CSRR. In this work, the latter case is selected due to observed higher Q-factors. When the gap is symmetric ($t_x = 0$), the ideal (lossless and infinite) structure supports a symmetry-protected BIC. If the central silicon gap is increased along the positive x direction, as defined in Fig. 1, the in-plane inversion symmetry is broken and BIC transforms into a quasi-BIC with a finite Q-factor.

Figure 4 shows the transmittance spectra of the substrate-supported MS studied in Fig. 2(a) for increasing values of the asymmetry parameter t_x. It is observed that when $t_x \neq 0$ a sharp quasi-BIC resonance manifests in the transmittance spectrum, whose λ_{res} and linewidth progressively increase for higher values of t_x. The resonant wavelength of the non-BIC mode at 1.5494 μm for $t_x = 0$ also red-shifts due to the increased volume occupied by silicon, as the asymmetry becomes more profound. The resonant electric and magnetic field of the quasi-BIC mode for the free-standing MS and for $t_x = 50$ nm and $\lambda_{\text{res}} = 1.53395$ μm calculated at the MS midplane are shown in Fig. 4(b). The electric (magnetic) field was found to be polarized exclusive in-plane (out-of-plane). The displacement currents demonstrate a circular pattern twisting around the center of the silicon surfaces bounded by the CSRR producing magnetic moments along the z-axis. A similar pattern has been identified as a collective oscillation of four longitudinal magnetic dipoles [83]. The CMDT analysis in Fig. 4(c) supports this ascertainment, as it reveals a predominant magnetic dipole contribution.

The investigated quasi-BIC resonant spectra have a Fano profile that can be studied with the classical Fano formula. However, in order to include the effect of absorption losses an extended Fano formula (Eq. (1)) for lossy two-port systems is here implemented [84]. This model embodies loss-related correction terms and fundamental parameters, namely resonance frequency, total decay rates, and partial radiation probabilities:

$$T(\omega_n) = \eta_{\text{rad}} T_{\text{Fano}}(\omega_n) - \beta \frac{\eta_{\text{rad}}\eta_{\text{abs}}}{1 + \left(\frac{\omega_n - 1}{\gamma_n}\right)^2} + \eta_{\text{abs}} |t_D|^2 , \tag{1}$$

Optics EXPRESS

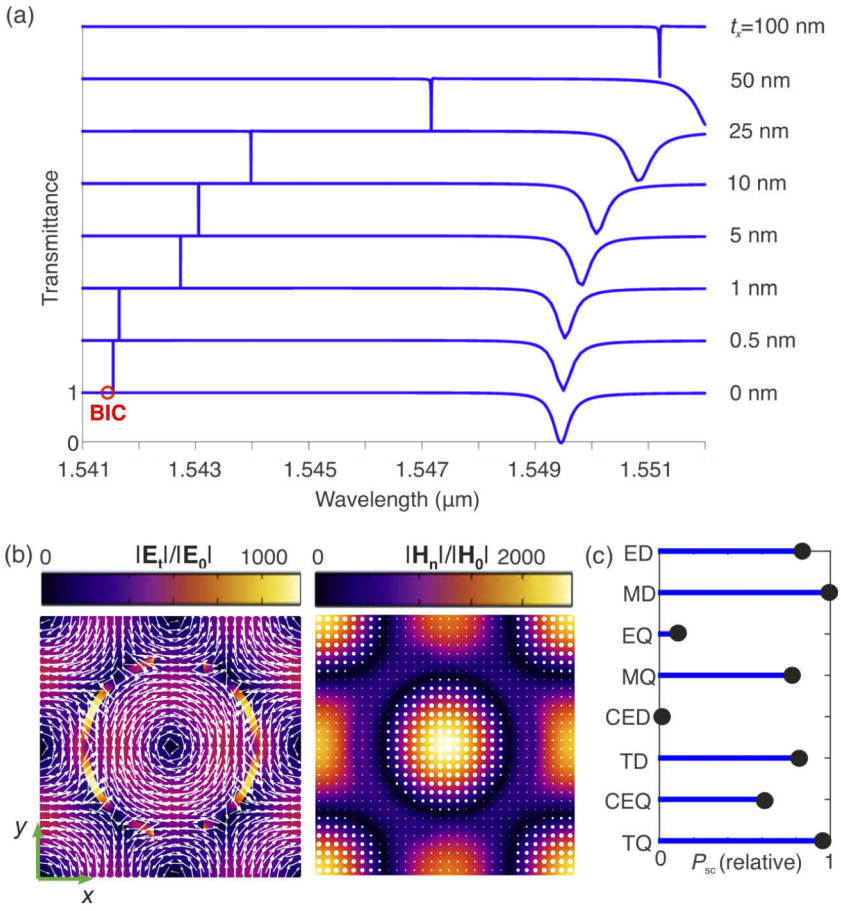

Fig. 4. (a) Transmittance of the substrate-supported MS for various values of the asymmetry parameter t_x; other parameters as in Fig. 2(a). (b) Tangential electric and normal magnetic field profiles at the xy-midplane of the MS for the corresponding free-standing MS and for t_x = 50 nm. (c) Relative multipole scattering power for the resonant quasi-BIC mode.

where $\eta_{\text{rad}} = 1 - \eta_{\text{abs}}$ is the total radiation probability of the localized mode, β is the intensity of the resonant transmission at the resonant wavelenght, t_D is the non-resonant transfer amplitude via the continuum, γ_n is the overall damping rate of the resonance ($Q = 1/2\gamma_n$), and T_{Fano} is the classic Fano formula

$$T_{\text{Fano}}(\omega_n) = |t_D|^2 \frac{(F\gamma_n + \omega_n - 1)^2}{(\omega_n - 1)^2 + \gamma_n^2}, \tag{2}$$

where $\omega_n = \omega/\omega_0$ is the normalized angular frequency, $\omega_0 = 2\pi f/\lambda_{\text{res}}$, λ_{res} is the resonant wavelength, F is the Fano parameter, expressing the degree of asymmetry. These parameters are obtained by curve fitting to the calculated transmittance spectra. Furthermore, in order to complement the results of the curve fitting to the extended Fano formula, we perform a FEM eigenfrequency analysis, calculating the quality factors of the quasi-BIC resonance as a function of the asymmetry parameter and losses in silicon as $Q = \Re\{\tilde{\omega}\}/2\Im\{\tilde{\omega}\}$, where $\tilde{\omega}$ is the calculated complex eigenfrequency.

Since optical glass substrates can be practically transparent, we focus our study on the optical losses in silicon, quantified by adding the extinction coefficient k, i.e., the imaginary part of the silicon refractive index. This coefficient encompasses both absorption and scattering

Optics EXPRESS

losses introduced by defects or due to surface roughness during fabrication. The results on the achievable Q-factors of the investigated quasi-BIC resonance are summarized in Fig. 5(a). Excellent agreement is observed between the Q-factor values derived by Fano fitting and those calculated by means of the eigenfrequency analysis. For the considered range of the asymmetry parameter ($t_x \geq 0.5$ nm), it was found that for $k<10^{-9}$, which is within the results of experimental characterization [60,85], the metasurface response is not affected. Larger values progressively deteriorate the Q-factor, as shown in Fig. 5(a) for $k = 10^{-5}$ and 10^{-7}, and reduce the transmission on resonance, as demonstrated in the spectra of Fig. 5(b) for $t_x = 1$ nm.

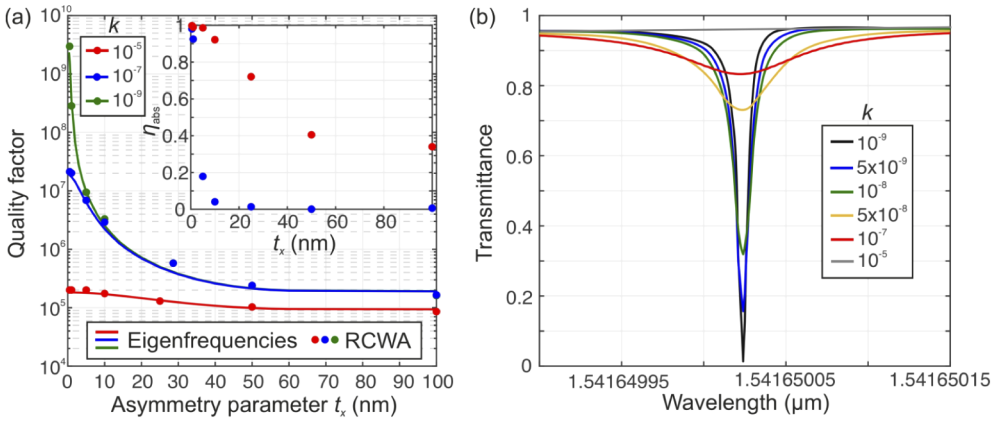

Fig. 5. (a) Quality factor of the quasi-BIC resonance in the CSRR-MS as a function the asymmetry parameter t_x and for three different extinction coefficients for losses in silicon ($k = 10^{-5}$, 10^{-7} and 10^{-9}). The inset shows the evolution of the absorption probability with t_x for two of the examined values of k. (b) Transmittance for different loss levels in the case $t_x = 1$ nm. The quasi-BIC resonance ceases to manifest for $k>10^{-5}$.

This effect can be quantified by the absorption probability η_{abs}. As this parameter increases, the contribution from T_{Fano} decreases linearly with the factor $\eta_{rad} = 1 - \eta_{abs}$ [84]. The value of the absorption probability as a function of the asymmetry parameter for $k = 10^{-5}$ and 10^{-7} is shown in the inset of Fig. 5(a). For $k = 10^{-9}$ the factor η_{abs} is negligible. In the case of lossless systems ($\eta_{rad} = 1$ and $\eta_{abs} = 0$), the transmittance is described by the standard Fano formula of Eq. (2), namely $T(\omega_n) = T_{Fano}(\omega_n)$. On the other hand, when the absorption probability is maximized, the resonance is fully quenched ($\eta_{rad} = 0$ and $\eta_{abs} = 1$), and $T(\omega_n) = |t_D|^2$. As observed in Fig. 5(b), for $t_x = 1$ nm and $k = 10^{-5}$, $\eta_{abs} = 1$ resulting in the suppression of the resonance. This analysis demonstrates the extreme sensitivity of quasi-BIC to losses and defects. On the other hand, this effect could be exploited to make active metasurfaces based on electro-optic or all-optic tuning of the carrier concentration in MS etched in doped silicon.

4. Conclusion

In summary, a CSRR silicon-slot dielectric metasurface exhibiting multipolar resonances and bound states in the continuum (BIC) was designed and demonstrated. The spectral position of these resonances is controlled by adjusting the structural parameters. The CSRR-based configuration of allows to have free-standing metasurfaces and produce an extra tuning parameter. Through proper design, the metasurface operates as an extremely narrowband notch filter. Thanks to the non-radiative nature of the resonances, the negligible absorption loss and the near field coupling on the metasurface, very high quality factors are demonstrated close to the telecom relevant wavelength of 1.55 μm, which are limited solely by fabrication tolerance and the control of absorption losses in silicon for the case of the quasi-BIC mode. The proposed structure can

Optics EXPRESS

find application in systems relying on strong light-matter interactions, such as non-linear devices, biological sensors, or on narrowband filtering, e.g., in laser cavities or optical communications.

Funding. Ministerio de Ciencia, Innovación y Universidades (PID2019-107270RB-C21, PID2019-109072RB-C31, RTC2017-6321-1); Comunidad de Madrid (S2018/NMT-4326); Ministerio de Economía y Competitividad (TEC2016-76021-C2-2-R, TEC2016-77242-C3-1-R).

Disclosures. The authors declare no conflicts of interest.

References

1. M. Kadic, G. W. Milton, M. van Hecke, and M. Wegener, "3D metamaterials," Nat. Rev. Phys. **1**(3), 198–210 (2019).
2. P. Qiao, W. Yang, and C. J. Chang-Hasnain, "Recent advances in high-contrast metastructures, metasurfaces, and photonic crystals," Adv. Opt. Photonics **10**(1), 180–245 (2018).
3. Y. Zhao and A. Alù, "Manipulating light polarization with ultrathin plasmonic metasurfaces," Phys. Rev. B **84**(20), 205428 (2011).
4. F. Aieta, P. Genevet, N. Yu, M. A. Kats, Z. Gaburro, and F. Capasso, "Out-of-plane reflection and refraction of light by anisotropic optical antenna metasurfaces with phase discontinuities," Nano Lett. **12**(3), 1702–1706 (2012).
5. N. Yu, F. Aieta, P. Genevet, M. A. Kats, Z. Gaburro, and F. Capasso, "A broadband, background-free quarter-wave plate based on plasmonic metasurfaces," Nano Lett. **12**(12), 6328–6333 (2012).
6. N. K. Grady, J. E. Heyes, D. R. Chowdhury, Y. Zeng, M. T. Reiten, A. K. Azad, A. J. Taylor, D. A. R. Dalvit, and H.-T. Chen, "Terahertz metamaterials for linear polarization conversion and anomalous refraction," Science **340**(6138), 1304–1307 (2013).
7. N. Meinzer, W. L. Barnes, and I. R. Hooper, "Plasmonic meta-atoms and metasurfaces," Nat. Photonics **8**(12), 889–898 (2014).
8. J. Algorri, B. García-Cámara, A. Cuadrado, J. Sánchez-Pena, and R. Vergaz, "Selective dielectric metasurfaces based on directional conditions of silicon nanopillars," Nanomaterials **7**(7), 177 (2017).
9. N. Yu, P. Genevet, M. A. Kats, F. Aieta, J.-P. Tetienne, F. Capasso, and Z. Gaburro, "Light propagation with phase discontinuities: Generalized laws of reflection and refraction," Science **334**(6054), 333–337 (2011).
10. X. Ni, N. K. Emani, A. V. Kildishev, A. Boltasseva, and V. M. Shalaev, "Broadband light bending with plasmonic nanoantennas," Science **335**(6067), 427 (2012).
11. S. Sun, K.-Y. Yang, C.-M. Wang, T.-K. Juan, W. T. Chen, C. Y. Liao, Q. He, S. Xiao, W.-T. Kung, G.-Y. Guo, L. Zhou, and D. P. Tsai, "High-efficiency broadband anomalous reflection by gradient meta-surfaces," Nano Lett. **12**(12), 6223–6229 (2012).
12. D. Lu and Z. Liu, "Hyperlenses and metalenses for far-field super-resolution imaging," Nat. Commun. **3**(1), 1205 (2012).
13. S. Wang, P. C. Wu, V.-C. Su, Y.-C. Lai, M.-K. Chen, H. Y. Kuo, B. H. Chen, Y. H. Chen, T.-T. Huang, J.-H. Wang, R.-M. Lin, C.-H. Kuan, T. Li, Z. Wang, S. Zhu, and D. P. Tsai, "A broadband achromatic metalens in the visible," Nat. Nanotechnol. **13**(3), 227–232 (2018).
14. S. Liu, A. Vaskin, S. Addamane, B. Leung, M.-C. Tsai, Y. Yang, P. P. Vabishchevich, G. A. Keeler, G. Wang, X. He, Y. Kim, N. F. Hartmann, H. Htoon, S. K. Doorn, M. Zilk, T. Pertsch, G. Balakrishnan, M. B. Sinclair, I. Staude, and I. Brener, "Light-emitting metasurfaces: Simultaneous control of spontaneous emission and far-field radiation," Nano Lett. **18**(11), 6906–6914 (2018).
15. A. Ferraro, D. C. Zografopoulos, M. A. Verschuuren, D. K. G. de Boer, F. Kong, H. P. Urbach, R. Beccherelli, and R. Caputo, "Directional emission of fluorescent dye-doped dielectric nanogratings for lighting applications," ACS Appl. Mater. Interfaces **10**(29), 24750–24757 (2018).
16. E. Arbabi, A. Arbabi, S. M. Kamali, Y. Horie, and A. Faraon, "Multiwavelength polarization-insensitive lenses based on dielectric metasurfaces with meta-molecules," Optica **3**(6), 628–633 (2016).
17. K. Ou, G. Li, T. Li, H. Yang, F. Yu, J. Chen, Z. Zhao, G. Cao, X. Chen, and W. Lu, "High efficiency focusing vortex generation and detection with polarization-insensitive dielectric metasurfaces," Nanoscale **10**(40), 19154–19161 (2018).
18. G.-D. Liu, X. Zhai, L.-L. Wang, Q. Lin, S.-X. Xia, X. Luo, and C.-J. Zhao, "A high-performance refractive index sensor based on fano resonance in si split-ring metasurface," Plasmonics **13**(1), 15–19 (2018).
19. J. Algorri, D. Zografopoulos, A. Ferraro, B. García-Cámara, R. Vergaz, R. Beccherelli, and J. Sánchez-Pena, "Anapole modes in hollow nanocuboid dielectric metasurfaces for refractometric sensing," Nanomaterials **9**(1), 30 (2018).
20. D. C. Zografopoulos, J. F. Algorri, A. Ferraro, B. García-Cámara, J. M. Sánchez-Pena, and R. Beccherelli, "Toroidal metasurface resonances in microwave waveguides," Sci. Rep. **9**(1), 7544 (2019).
21. J. Algorri, D. Zografopoulos, A. Ferraro, B. García-Cámara, R. Beccherelli, and J. Sánchez-Pena, "Ultrahigh-quality factor resonant dielectric metasurfaces based on hollow nanocuboids," Opt. Express **27**(5), 6320–6330 (2019).
22. S. Campione, S. Liu, L. I. Basilio, L. K. Warne, W. L. Langston, T. S. Luk, J. R. Wendt, J. L. Reno, G. A. Keeler, I. Brener, and M. B. Sinclair, "Broken symmetry dielectric resonators for high quality factor Fano metasurfaces," ACS Photonics **3**(12), 2362–2367 (2016).
23. Y. Yang, I. I. Kravchenko, D. P. Briggs, and J. Valentine, "All-dielectric metasurface analogue of electromagnetically induced transparency," Nat. Commun. **5**(1), 5753 (2014).

Optics EXPRESS

24. S. Liu, M. B. Sinclair, S. Saravi, G. A. Keeler, Y. Yang, J. Reno, G. M. Peake, F. Setzpfandt, I. Staude, T. Pertsch, and I. Brener, "Resonantly enhanced second-harmonic generation using III-V semiconductor all-dielectric metasurfaces," Nano Lett. **16**(9), 5426–5432 (2016).
25. P. P. Vabishchevich, S. Liu, M. B. Sinclair, G. A. Keeler, G. M. Peake, and I. Brener, "Enhanced second-harmonic generation using broken symmetry III-V semiconductor Fano metasurfaces," ACS Photonics **5**(5), 1685–1690 (2018).
26. N. Yu and F. Capasso, "Flat optics with designer metasurfaces," Nat. Mater. **13**(2), 139–150 (2014).
27. S. B. Glybovski, S. A. Tretyakov, P. A. Belov, Y. S. Kivshar, and C. R. Simovski, "Metasurfaces: From microwaves to visible," Phys. Rep. **634**, 1–72 (2016).
28. A. Y. Zhu, A. I. Kuznetsov, B. Luk'yanchuk, N. Engheta, and P. Genevet, "Traditional and emerging materials for optical metasurfaces," Nanophotonics **6**(2), 452–471 (2017).
29. P. Genevet, F. Capasso, F. Aieta, M. Khorasaninejad, and R. Devlin, "Recent advances in planar optics: from plasmonic to dielectric metasurfaces," Optica **4**(1), 139–152 (2017).
30. D. Lee, J. Gwak, T. Badloe, S. Palomba, and J. Rho, "Metasurfaces-based imaging and applications: from miniaturized optical components to functional imaging platforms," Nanoscale Adv. **2**(2), 605–625 (2020).
31. V. A. Fedotov, M. Rose, S. L. Prosvirnin, N. Papasimakis, and N. I. Zheludev, "Sharp trapped-mode resonances in planar metamaterials with a broken structural symmetry," Phys. Rev. Lett. **99**(14), 147401 (2007).
32. A. B. Evlyukhin and B. N. Chichkov, "Multipole decompositions for directional light scattering," Phys. Rev. B **100**(12), 125415 (2019).
33. E. A. Gurvitz, K. S. Ladutenko, P. A. Dergachev, A. B. Evlyukhin, A. E. Miroshnichenko, and A. S. Shalin, "The high-order toroidal moments and anapole states in all-dielectric photonics," Laser Photonics Rev. **13**(5), 1800266 (2019).
34. P. D. Terekhov, V. E. Babicheva, K. V. Baryshnikova, A. S. Shalin, A. Karabchevsky, and A. B. Evlyukhin, "Multipole analysis of dielectric metasurfaces composed of nonspherical nanoparticles and lattice invisibility effect," Phys. Rev. B **99**(4), 045424 (2019).
35. S. Xu, A. Sayanskiy, A. S. Kupriianov, V. R. Tuz, P. Kapitanova, H.-B. Sun, W. Han, and Y. S. Kivshar, "Experimental observation of toroidal dipole modes in all-dielectric metasurfaces," Adv. Opt. Mater. **7**(4), 1801166 (2018).
36. R. Alaee, C. Rockstuhl, and I. Fernandez-Corbaton, "An electromagnetic multipole expansion beyond the long-wavelength approximation," Opt. Commun. **407**, 17–21 (2018).
37. R. Alaee, C. Rockstuhl, and I. Fernandez-Corbaton, "Exact multipolar decompositions with applications in nanophotonics," Adv. Opt. Mater. **7**(1), 1800783 (2019).
38. P. D. Terekhov, A. B. Evlyukhin, D. Redka, V. S. Volkov, A. S. Shalin, and A. Karabchevsky, "Magnetic octupole response of dielectric quadrumers," Laser Photonics Rev. **14**(4), 1900331 (2020).
39. C. Zhou, S. Li, Y. Wang, and M. Zhan, "Multiple toroidal dipole Fano resonances of asymmetric dielectric nanohole arrays," Phys. Rev. B **100**(19), 195306 (2019).
40. T. Kaelberer, V. A. Fedotov, N. Papasimakis, D. P. Tsai, and N. I. Zheludev, "Toroidal dipolar response in a metamaterial," Science **330**(6010), 1510–1512 (2010).
41. X. Chen and W. Fan, "Study of the interaction between graphene and planar terahertz metamaterial with toroidal dipolar resonance," Opt. Lett. **42**(10), 2034 (2017).
42. P. C. Wu, C. Y. Liao, V. Savinov, T. L. Chung, W. T. Chen, Y.-W. Huang, P. R. Wu, Y.-H. Chen, A.-Q. Liu, N. I. Zheludev, and D. P. Tsai, "Optical anapole metamaterial," ACS Nano **12**(2), 1920–1927 (2018).
43. A. E. Miroshnichenko, A. B. Evlyukhin, Y. F. Yu, R. M. Bakker, A. Chipouline, A. I. Kuznetsov, B. Luk'yanchuk, B. N. Chichkov, and Y. S. Kivshar, "Nonradiating anapole modes in dielectric nanoparticles," Nat. Commun. **6**(1), 8069 (2015).
44. A. Sayanskiy, M. Danaeifar, P. Kapitanova, and A. E. Miroshnichenko, "All-dielectric metalattice with enhanced toroidal dipole response," Adv. Opt. Mater. **6**(19), 1800302 (2018).
45. D. C. Zografopoulos, A. Ferraro, J. F. Algorri, P. Martín-Mateos, B. García-Cámara, A. Moreno-Oyervides, V. Krozer, P. Acedo, R. Vergaz, J. M. Sánchez-Pena, and R. Beccherelli, "All-dielectric silicon metasurface with strong subterahertz toroidal dipole resonance," Adv. Opt. Mater. **7**(19), 1900777 (2019).
46. A. K. Ospanova, G. Labate, L. Matekovits, and A. A. Basharin, "Multipolar passive cloaking by nonradiating anapole excitation," Sci. Rep. **8**(1), 12514 (2018).
47. J. S. T. Gongora, A. E. Miroshnichenko, Y. S. Kivshar, and A. Fratalocchi, "Anapole nanolasers for mode-locking and ultrafast pulse generation," Nat. Commun. **8**(1), 15535 (2017).
48. C. Cui, S. Yuan, X. Qiu, L. Zhu, Y. Wang, Y. Li, J. Song, Q. Huang, C. Zeng, and J. Xia, "Light emission driven by magnetic and electric toroidal dipole resonances in a silicon metasurface," Nanoscale **11**(30), 14446–14454 (2019).
49. G. Grinblat, Y. Li, M. P. Nielsen, R. F. Oulton, and S. A. Maier, "Efficient third harmonic generation and nonlinear subwavelength imaging at a higher-order anapole mode in a single germanium nanodisk," ACS Nano **11**(1), 953–960 (2017).
50. M. Timofeeva, L. Lang, F. Timpu, C. Renaut, A. Bouravleuv, I. Shtrom, G. Cirlin, and R. Grange, "Anapoles in free-standing III-V nanodisks enhancing second-harmonic generation," Nano Lett. **18**(6), 3695–3702 (2018).
51. N. Papasimakis, V. A. Fedotov, V. Savinov, T. A. Raybould, and N. I. Zheludev, "Electromagnetic toroidal excitations in matter and free space," Nat. Mater. **15**(3), 263–271 (2016).
52. V. Savinov, N. Papasimakis, D. P. Tsai, and N. I. Zheludev, "Optical anapoles," Commun. Phys. **2**(1), 69 (2019).

Optics EXPRESS

53. A. Ahmadivand, B. Gerislioglu, R. Ahuja, and Y. K. Mishra, "Toroidal metaphotonics and metadevices," Laser Photonics Rev. **14**(11), 1900326 (2020).
54. Y. F. Yu, A. Y. Zhu, R. Paniagua-Domínguez, Y. H. Fu, B. Luk'yanchuk, and A. I. Kuznetsov, "High-transmission dielectric metasurface with 2π phase control at visible wavelengths," Laser Photonics Rev. **9**(4), 412–418 (2015).
55. P. A. Jeong, M. D. Goldflam, S. Campione, J. L. Briscoe, P. P. Vabishchevich, J. Nogan, M. B. Sinclair, T. S. Luk, and I. Brener, "High quality factor toroidal resonances in dielectric metasurfaces," ACS Photonics **7**(7), 1699–1707 (2020).
56. J. Hugonin and P. Lalanne, "RETICOLO software for grating analysis, Institut d'Optique, Orsay, France," (2005).
57. P. Lalanne and G. M. Morris, "Highly improved convergence of the coupled-wave method for TM polarization," J. Opt. Soc. Am. A **13**(4), 779 (1996).
58. P. Lalanne and M. P. Jurek, "Computation of the near-field pattern with the coupled-wave method for transverse magnetic polarization," J. Mod. Opt. **45**(7), 1357–1374 (1998).
59. J. Jiang, R. Lupoiu, E. W. Wang, D. Sell, J. P. Hugonin, P. Lalanne, and J. A. Fan, "MetaNet: a new paradigm for data sharing in photonics research," Opt. Express **28**(9), 13670 (2020).
60. M. A. Green, "Self-consistent optical parameters of intrinsic silicon at 300 K including temperature coefficients," Sol. Energy Mater. Sol. Cells **92**(11), 1305–1310 (2008).
61. J. von Neumann and E. P. Wigner, "Über merkwürdige diskrete eigenwerte," in *The Collected Works of Eugene Paul Wigner*, (Springer Berlin Heidelberg, 1993), pp. 291–293.
62. C. W. Hsu, B. Zhen, A. D. Stone, J. D. Joannopoulos, and M. Soljačić, "Bound states in the continuum," Nat. Rev. Mater. **1**(9), 16048 (2016).
63. Y. Plotnik, O. Peleg, F. Dreisow, M. Heinrich, S. Nolte, A. Szameit, and M. Segev, "Experimental observation of optical bound states in the continuum," Phys. Rev. Lett. **107**(18), 183901 (2011).
64. Z. F. Sadrieva, I. S. Sinev, K. L. Koshelev, A. Samusev, I. V. Iorsh, O. Takayama, R. Malureanu, A. A. Bogdanov, and A. V. Lavrinenko, "Transition from optical bound states in the continuum to leaky resonances: Role of substrate and roughness," ACS Photonics **4**(4), 723–727 (2017).
65. C. W. Hsu, B. Zhen, J. Lee, S.-L. Chua, S. G. Johnson, J. D. Joannopoulos, and M. Soljačić, "Observation of trapped light within the radiation continuum," Nature **499**(7457), 188–191 (2013).
66. Y. Yang, C. Peng, Y. Liang, Z. Li, and S. Noda, "Analytical perspective for bound states in the continuum in photonic crystal slabs," Phys. Rev. Lett. **113**(3), 037401 (2014).
67. S. T. Ha, Y. H. Fu, N. K. Emani, Z. Pan, R. M. Bakker, R. Paniagua-Domínguez, and A. I. Kuznetsov, "Directional lasing in resonant semiconductor nanoantenna arrays," Nat. Nanotechnol. **13**(11), 1042–1047 (2018).
68. X. Yin, J. Jin, M. Soljačić, C. Peng, and B. Zhen, "Observation of topologically enabled unidirectional guided resonances," Nature **580**(7804), 467–471 (2020).
69. E. Bulgakov and A. Sadreev, "Fibers based on propagating bound states in the continuum," Phys. Rev. B **98**(8), 085301 (2018).
70. X. Gao, B. Zhen, M. Soljačić, H. Chen, and C. W. Hsu, "Bound states in the continuum in fiber bragg gratings," ACS Photonics **6**(11), 2996–3002 (2019).
71. A. Forouzmand and H. Mosallaei, "All-dielectric c-shaped nanoantennas for light manipulation: Tailoring both magnetic and electric resonances to the desire," Adv. Opt. Mater. **5**(14), 1700147 (2017).
72. A. Tittl, A. Leitis, M. Liu, F. Yesilkoy, D.-Y. Choi, D. N. Neshev, Y. S. Kivshar, and H. Altug, "Imaging-based molecular barcoding with pixelated dielectric metasurfaces," Science **360**(6393), 1105–1109 (2018).
73. Y. He, G. Guo, T. Feng, Y. Xu, and A. E. Miroshnichenko, "Toroidal dipole bound states in the continuum," Phys. Rev. B **98**(16), 161112 (2018).
74. A. S. Kupriianov, Y. Xu, A. Sayanskiy, V. Dmitriev, Y. S. Kivshar, and V. R. Tuz, "Metasurface engineering through bound states in the continuum," Phys. Rev. Appl. **12**(1), 014024 (2019).
75. M. V. Rybin, K. L. Koshelev, Z. F. Sadrieva, K. B. Samusev, A. A. Bogdanov, M. F. Limonov, and Y. S. Kivshar, "High-Q supercavity modes in subwavelength dielectric resonators," Phys. Rev. Lett. **119**(24), 243901 (2017).
76. S. Li, C. Zhou, T. Liu, and S. Xiao, "Symmetry-protected bound states in the continuum supported by all-dielectric metasurfaces," Phys. Rev. A **100**(6), 063803 (2019).
77. S. Romano, G. Zito, S. Torino, G. Calafiore, E. Penzo, G. Coppola, S. Cabrini, I. Rendina, and V. Mocella, "Label-free sensing of ultralow-weight molecules with all-dielectric metasurfaces supporting bound states in the continuum," Photonics Res. **6**(7), 726 (2018).
78. S. Romano, G. Zito, S. N. L. Yépez, S. Cabrini, E. Penzo, G. Coppola, I. Rendina, and V. Mocellaark, "Tuning the exponential sensitivity of a bound-state-in-continuum optical sensor," Opt. Express **27**(13), 18776 (2019).
79. Z. Liu, Y. Xu, Y. Lin, J. Xiang, T. Feng, Q. Cao, J. Li, S. Lan, and J. Liu, "High-Q quasibound states in the continuum for nonlinear metasurfaces," Phys. Rev. Lett. **123**(25), 253901 (2019).
80. C. Zhou, X. Qu, S. Xiao, and M. Fan, "Imaging through a Fano-resonant dielectric metasurface governed by quasi–bound states in the continuum," Phys. Rev. Appl. **14**(4), 044009 (2020).
81. A. Kodigala, T. Lepetit, Q. Gu, B. Bahari, Y. Fainman, and B. Kanté, "Lasing action from photonic bound states in continuum," Nature **541**(7636), 196–199 (2017).
82. K. Koshelev, S. Lepeshov, M. Liu, A. Bogdanov, and Y. Kivshar, "Asymmetric metasurfaces with high-Q resonances governed by bound states in the continuum," Phys. Rev. Lett. **121**(19), 193903 (2018).

Optics EXPRESS

83. V. R. Tuz, V. V. Khardikov, and Y. S. Kivshar, "All-dielectric resonant metasurfaces with a strong toroidal response," ACS Photonics **5**(5), 1871–1876 (2018).
84. J. W. Yoon and R. Magnusson, "Fano resonance formula for lossy two-port systems," Opt. Express **21**(15), 17751 (2013).
85. C. Schinke, P. C. Peest, J. Schmidt, R. Brendel, K. Bothe, M. R. Vogt, I. Kröger, S. Winter, A. Schirmacher, S. Lim, H. T. Nguyen, and D. MacDonald, "Uncertainty analysis for the coefficient of band-to-band absorption of crystalline silicon," AIP Adv. **5**(6), 067168 (2015).